A&A 520, A73 (2010)
DOI: 10.1051/0004-6361/201014096

Astronomy & Astrophysics

V945 Centauri = HD 112409: a bright hot short-period binary in a triple system?⋆,⋆⋆

P. Harmanec[1], C. Aerts[2,3], A. Prša[4,5], T. Verhoelst[2,⋆⋆⋆], and K. Kolenberg[2,6]

[1] Astronomical Institute of the Charles University, Faculty of Mathematics and Physics, V Holešovičkách 2, 180 00 Praha 8, Czech Republic
e-mail: hec@sirrah.troja.mff.cuni.cz
[2] Instituut voor Sterrenkunde, Katholieke Universiteit Leuven, Celestijnenlaan 200 D, 3001 Leuven, Belgium
[3] Department of Astrophysics, IMAPP, Radboud University Nijmegen, PO Box 9010, 6500 GL Nijmegen, The Netherlands
[4] Villanova University, Dept. of Astronomy & Astrophysics, 800 Lancaster Ave, Villanova, PA 19085, USA
[5] University of Ljubljana, Dept. of Physics, Jadranska 19, 1000 Ljubljana, Slovenia
[6] Institut für Astronomie, Universität Wien, Türkenschanzstrasse 17, 1180 Wien, Austria

Received 19 January 2010 / Accepted 24 May 2010

ABSTRACT

A detailed analysis of multicolour Geneva photometry and high-resolution echelle spectroscopy of the B8.5V star V945 Cen (HD 112409, $V = 5\overset{\mathrm{m}}{.}2$) whose short-term periodic variability was first detected from the HIPPARCOS data, led to the finding that the object is an ellipsoidal variable and a close double-lined spectroscopic binary with a $0\overset{\mathrm{d}}{.}6496$ orbital period and a circular orbit. The components have spectral types B7 and B8.5 and are both main-sequence objects. The system is detached but close to a contact configuration and is observed at an inclination of ~23–24°. A notable finding is that the optical spectrum also contains a third system of spectral lines corresponding to a late B spectral type that remained stationary during the 5 days of spectral observations. From several independent lines of reasoning, we tentatively conclude that the third spectrum belongs to a real third body in the system. However, the possibility that it instead originates in circumbinary gas cannot be excluded completely, and additional spectral and interferometric observations are required to help us determine its origin conclusively.

Key words. binaries: close – stars: variables: general – stars: individual: V945 Cen = HD 112409

1. Introduction

The success of the ESA HIPPARCOS mission led, among other things, to discoveries of many new variables (Eyer & Grenon 1997; Kazarovets et al. 1999). Waelkens et al. (1998) attempted to classify the periodically variable B stars among them. The star V945 Cen (HD 112409), a bright ($V = 5\overset{\mathrm{m}}{.}2$) B8.5V variable with a period of some 8 h is on their list. This short-period light variability may be caused by several phenomena: (1) by a non-radial gravity mode as in the slowly pulsating B stars (De Cat & Aerts 2002); (2) by rotational modulation in chemically peculiar B stars (Briquet et al. 2004); (3) by duplicity of the star in question (De Cat et al. 2000); or (4) by a combination of several of the first three possibilities. Waelkens et al. (1998) tentatively classified V945 Cen as a slowly pulsating B star.

Aerts et al. (1999) and Mathias et al. (2001) carried out extended long-term photometric and spectroscopic follow-up studies of the new candidates for slowly pulsating B stars including V945 Cen. Since the spectroscopic monitoring was carried out mainly in a region centered on the Si II 4128 nad 4130 Å doublet, their preference was to study mainly the stars with low $v \sin i$ values, for which this doublet is not blended. Therefore, V945 Cen was not initially spectroscopically observed because of its rather large $v \sin i = 164$ km s^{-1} (Brown & Verschueren 1997). However, since this star was one of very few additional B8–9 IV–V candidates to enlarge the group of slowly pulsating B stars, a separate spectroscopic 5-day campaign was carried out by the Leuven team to search for possible line-profile variations in three of these stars, using échelle spectra which covered a wide range of wavelengths. The results for HD 121190 and HD 106419 have already been published elsewhere (Aerts & Kolenberg 2005) and indeed confirmed the classification of these two objects as pulsating stars. For V945 Cen, however, clear evidence of ellipsoidal variations in a double-lined close binary with an orbital period of some 16 h was found.

We present the results of a detailed study of this newly discovered bright binary. Its B spectral type and short orbital period make V945 Cen an astrophysically very interesting system. The binary has not yet been the topic of a detailed study, its very short orbital period qualifying it as a candidate for a case A mass exchange. However, in contrast to other such systems discussed in the literature, this object is not an eclipsing binary. One therefore has a unique chance to compare the observed properties of the binary seen more pole-on with its counterparts observed roughly equator-on.

2. Observational data

2.1. Multicolour Geneva and Hipparcos H_p photometry

We refer readers to Aerts & Kolenberg (2005) for a general description of the photometric monitoring programme at Leuven University in which V945 Cen was included.

⋆ Based on photometry gathered with the Swiss 0.7-m telescope equipped with the P7 photometer of the Geneva Observatory and on spectroscopy assembled with the FEROS spectrograph attached to the ESO 2.2 m telescope, both situated at La Silla in Chile.

⋆⋆ Reduced data is only available in electronic form at the CDS via anonymous ftp to cdarc.u-strasbg.fr (130.79.128.5) or via http://cdsarc.u-strasbg.fr/viz-bin/qcat?J/A+A/520/A73

⋆⋆⋆ Postdoctoral Fellow of the Fund for Scientific Research, Flanders.

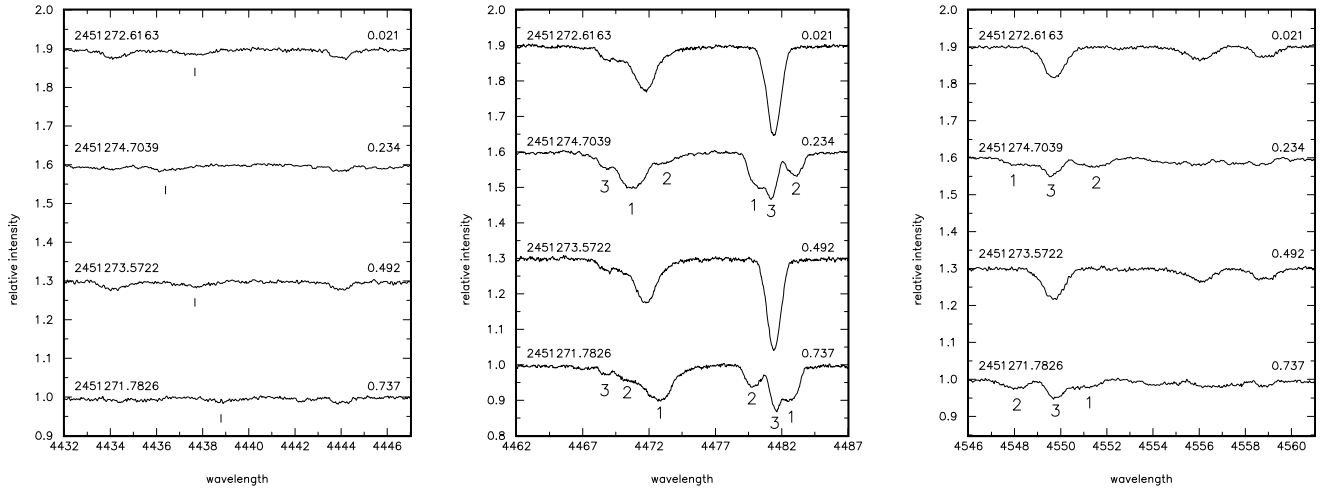

Fig. 1. Four segments of the spectra containing some interesting spectral lines. Heliocentric Julian dates and orbital phases of the spectra are given in each panel. For clarity, the continua of subsequent spectra are shifted by 0.3 units in normalized intensity. *The left panel* shows the region near the He I 4437.551 Å line (the position of which is shown by a bar), the central panel shows the neighbourhood of He I 4471.508 Å and Mg II 4481.228 Å, and the right one shows the Fe II 4549 Å line. It is obvious that the observed spectrum is actually a combination of three different spectra, identified as components 1, 2, and 3 for the spectra taken at both elongations of the 0.65-d binary. Note, however, that the line of component 3 to the left of the He I 4471.508 Å line is Ti II 4468.507 Å. See the text for details.

We obtained Geneva 7-colour high-precision photometry of V945 Cen during one campaign of 3-week duration and one campaign of 9 weeks within one season. The data were obtained with the photometer P 7 attached to the 0.7 m Swiss telescope situated at La Silla Observatory. Each datapoint is the result of averaging three consecutive exposures of 40 s. The corrections for the sky were carried out by observing at least two standard stars per hour at the same airmass as the target. The Geneva database consists of thousands of measurements gathered at La Silla between 1973 and 1997, which underwent a very accurate global calibration by means of all standard star measurements taken over 25 years. The system is so stable that data taken decades apart can easily be combined (see, e.g., De Cat & Aerts 2002; and Aerts et al. 2003a, for examples). These global reductions lead to a precision of about 5 mmag per measurement for V945 Cen. We obtained 160 observations over a time span of 121 days. We also had 5 very old Geneva observations secured some 20 years earlier. These observations are fully compatible with the new ones, therefore we also used them in the analysis. All individual observations with their HJDs are in Table 1, published electronically in CDS.

Additionally, we also used all HIPPARCOS H_p broad-band photometric observations with error flags 0 and 1 (Perryman & ESA 1997). To the best of our knowledge, there are no other published photometric observations of this object with known mid-exposure times.

2.2. High-resolution spectroscopy

A series of high-S/N spectra was obtained with the FEROS échelle spectrograph attached to the ESO 2.2 m telescope. The data were secured during 5 consecutive nights 2 years after the photometric campaigns. Integration times 8–15 min were used, depending on the atmospheric conditions. This resulted in S/N of 300–600 in the blue region of the spectrum. All spectra were reduced with standard routines available in the ESO software package MIDAS. They included tasks to deal with sky background subtraction, flatfielding, and wavelength calibration using Th-Ar spectra. The final rectification and removal of cosmics and flaws was carried out independently by CA in MIDAS and by PH in SPEFO (Horn et al. 1996; Škoda 1996). The original spectra are now freely available in the FEROS archive maintained by ESO.

We searched for strong enough, isolated lines free of line blending caused by rapid rotation. This is the case for the Mg II 4481.129 Å and the Si II 6347.109 Å lines. We also considered the C II doublet at 6578.053 and 6582.882 Å. However, these C II lines were found to be unusable for a detailed line-profile analysis because of their very limited strength and blending. No emission is seen in the Hα line, though faint emission may escape detection because of the complicated line profile with three overlapping absorption components. Given the spectral classification, we also searched for the He I lines. Rather surprisingly, one observes not only strong lines such as the He I 4471.473 Å line and He I 6678.151 Å line, but also the weak He I 4437.551 Å line, which is usually only observed in chemically peculiar He strong stars.

In Fig. 1, interesting segments of four selected blue spectra from both conjunctions and elongations of the binary are shown. One can clearly see three separate line components at certain orbital phases and only one deep line, a blend of all components, at other phases in the Mg II 4481 Å and Fe II 4549 Å lines. It is also seen that components 1 and 2 interchange their position as the stars move in the binary orbit, while component 3 appears stationary over the five days of our observations. The Balmer, Fe II, and Si II lines contain obvious contributions from all three components, while the He I 4437 and 6678 Å seem to be observable only as single lines. We will discuss the radial-velocity (RV hereafter) variations of all three components (which we denote 1, 2, and 3 in some panels of Fig. 1) in the following section.

A journal of all the new photometric and spectroscopic data is provided in Table 2.

2.3. The spectral energy distribution

As in the case of many bright B-type objects (Waters et al. 1987), V945 Cen is an IRAS source. The IRAS satellite only measured

Table 2. Journal of photometric and spectroscopic observations.

Photometry		Spectroscopy	
Time interval (HJD-2 400 000)	No. of obs.	Time interval (HJD-2 400 000)	No. of obs.
43 655.6–44 298.7	5	51 270.7–51 270.9	9
50 480.8–50 503.7	29	51 271.7–51 271.8	4
50 541.7–50 601.6	131	51 272.5–51 272.9	11
47 868.5–49 039.5	189	51 273.5–51 273.9	11
		51 274.5–51 274.9	9

Notes. The first three photometric data sets refer to Geneva photometry, the last one to the Hipparcos H_p observations.

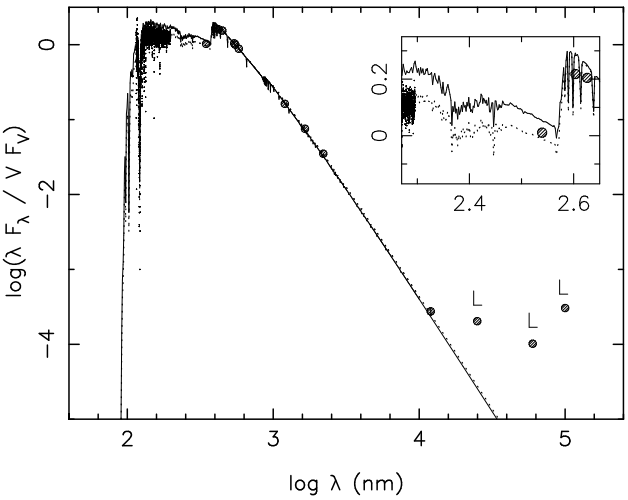

Fig. 2. The observed spectral energy distribution of V945 Cen (circles denoting the measurements in various passbands plus a plot of the IUE spectrum) is compared to that from a Kurucz model atmosphere for $T_{\rm eff}$ = 13 000 K and $\log g$ = 4.0 (solid line) and to a combined energy distribution resulting from a sum of relative contributions of three stars being represented by the same model as before for the primary ($T_{\rm eff}$ = 13 000, $\log g$ = 4.0) and a model with $T_{\rm eff}$ = 11 000, and $\log g$ = 4.0 for the secondary and tertiary (dotted line). The "L" symbols indicate only upper limits to the IRAS flux.

reliable infrared flux at 12 μm, while the values detected at 25, 60, and 100 μm are *only upper limits*. The IUE archive contains one high-dispersion spectrum of V945 Cen obtained with a large aperture, SWP 27531 from January 1986.

We constructed a spectral energy distribution (SED) from our Geneva data, the 2MASS catalogue, and the IRAS and IUE fluxes, applying a proper colour correction. This observed distribution was subsequently compared with Kurucz atmosphere models (Kurucz 1979). At first, we compared the data with an LTE atmosphere for $T_{\rm eff}$ = 13 000 K and $\log g$ = 4.0. This model is shown as a full line in Fig. 2.

Since three line components were discovered in the spectrum, we also constructed an SED by combining three atmosphere models and using their relative flux ratios obtained from our final modeling (see Table 6). This combined SED, shown by a dotted line in Fig. 2, is in closer agreement with the observed one.

The absence of any detectable infrared excess at 12 μm means that we cannot be dealing with dust formation. The absence of any detectable Balmer emission in the observed spectra also implies that a circumbinary envelope is probably not the source of the third spectrum. We therefore tentatively conclude that the third line spectrum originates from a real third body in the system.

2.4. NAOS-CONICA observations

On 27 January 2005, V945 Cen was observed with the adaptive optics instrument NAOS-CONICA on the VLT (Lenzen et al. 2003; Rousset et al. 2003). The observations were performed with the K_s band filter (λ_c = 2.18 μm) and a 27.053 milliarcsec (mas) pixel scale, yielding a total field-of-view of 28 × 28 arcseconds (1024 × 1024 pixels).

The images display only a single object, to intensities lower than 0.1% of the peak flux, within a 14 arcsec radius. This object appears unresolved with a *FWHM* of roughly 95 mas, which is similar to the PSF observations. Regrettably, these observations provided no direct evidence of a third body in the system.

3. The character and period of the variations

3.1. Photometry

The photometric data clearly exhibit a dominant frequency of 3.0796 c d^{-1} (P = 0$^{\rm d}$.32472), which is entirely compatible with, but differs slightly from the result found from the HIPPARCOS photometry (3.07882 c d^{-1}; P = 0$^{\rm d}$.324800). A very significant peak also occurs at a half of this frequency, which is the next maximum to be found in the periodograms after prewhitening in each of the datasets. This result is independent of the frequency search algorithm adopted and is consistent for all the seven Geneva filters and the HIPPARCOS data. We therefore interpret the detected dominant frequency as a half of the physical frequency controlling the variations. An analysis of RV data (see the next section) confirmed this and indicated that the star is indeed an ellipsoidal variable and a spectroscopic binary. The deeper and slightly shallower minima of all the light curves are separated by exactly one half of the orbital period, which is indicative of a circular orbit. This is unsurprising for such a short period.

All additional tests led to the conclusion that all photometric data can be reconciled with a single period of about 0$^{\rm d}$.64960. Within the limits of accuracy of the available observations, there is no evidence of a secular change in the period. From the final modelling discussed in Sect. 4, we derived the following binary ephemeris

$$T_{\rm min.\,I} = {\rm HJD}\,2\,450\,545.7081 + 0^{\rm d}.649593 \times E. \quad (1)$$

We show the phase plots for both the Geneva V magnitude and the Hipparcos H_p magnitude in Fig. 3. One can see that the variations are indeed typical of ellipsoidal variables. Inspecting the light curves in all passbands, we note that the difference in the relative depth of the primary and secondary minima decreases from U to V (cf. Fig. 10 below).

3.2. Spectroscopy

To understand the origin of the three line components 1, 2, and 3 seen in Fig. 1, we first measured their RVs in a classical way using SPEFO. SPEFO displays direct and reverse traces of the line profiles superimposed on the computer screen that the user can slide to achieve a precise overlapping of the chosen parts of the profile. We tried to measure several clean, unblended lines but we had to skip some spectra near the binary conjunctions where the line profiles from the primary and secondary were blended.

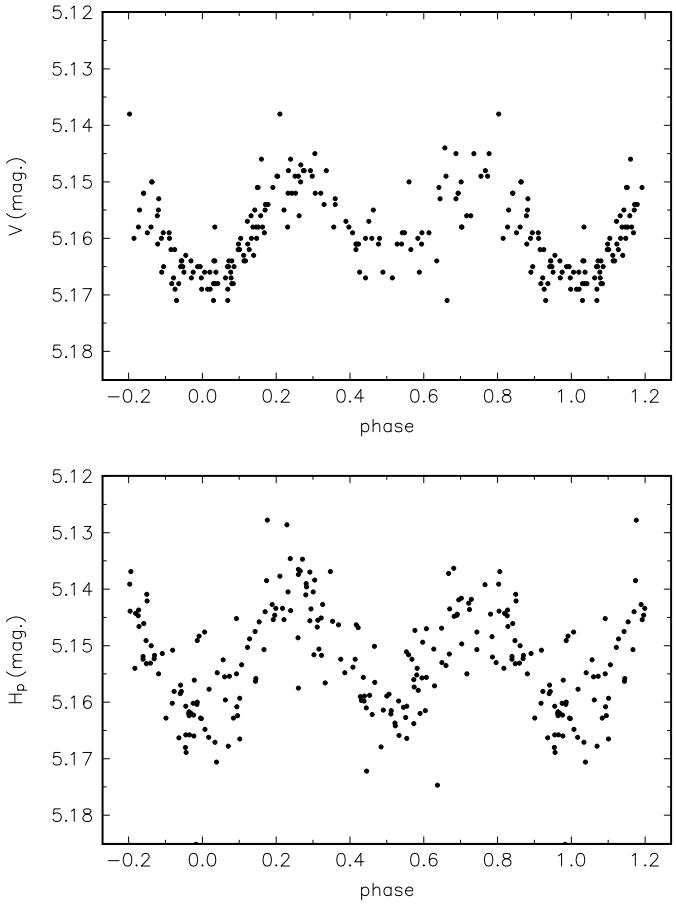

Fig. 3. A phase plot for the Geneva V (*upper panel*) and Hipparcos H_p (*lower panel*) photometry. Ephemeris (1) was used.

From these classical RV measurements (plotted versus orbital phase in Fig. 4), it became obvious that component 1 follows the RV curve of the star, which is in the upper (superior) conjunction at the primary minimum of the light curve, while component 2 moves in orbit with the other star. From now on, we refer to these two stars as the primary and the secondary, respectively.

The RV of component 3, first measured for a few strong lines, also seemed to vary in phase with the primary but with a much lower semi-amplitude of a few km s^{-1} only. However, it was then unclear whether this was a spurious effect caused by line blending. This suspicion was increased by our SPEFO measurement of the RV of the sharp Hα core (see Fig. 5). It appears that the RV of the Hα core varies in phase with component 1 but also with a reduced amplitude. Moreover, an oscillation with a resonant period of one third of the orbital one is detected. We demonstrate in the Appendix that this Hα variation is spurious. Since both binary components have Hα profiles with sharp cores and broad wings, they inevitably blend with the stationary sharp component 3 as they move in orbit around each other. This, together with the relative intensity variations explains the artifact. Indeed, when we measured the RV of the Ti II 4443.794 Å line, its RV was found to be *constant* within the limits of the accuracy of its measurement (-11.8 ± 3.6 km s^{-1}) and to show no obvious phase dependence on the orbital phase (see the bottom panel of Fig. 4). Since the effect of the line blending in the Hα line is interesting and our finding represents a methodological warning,

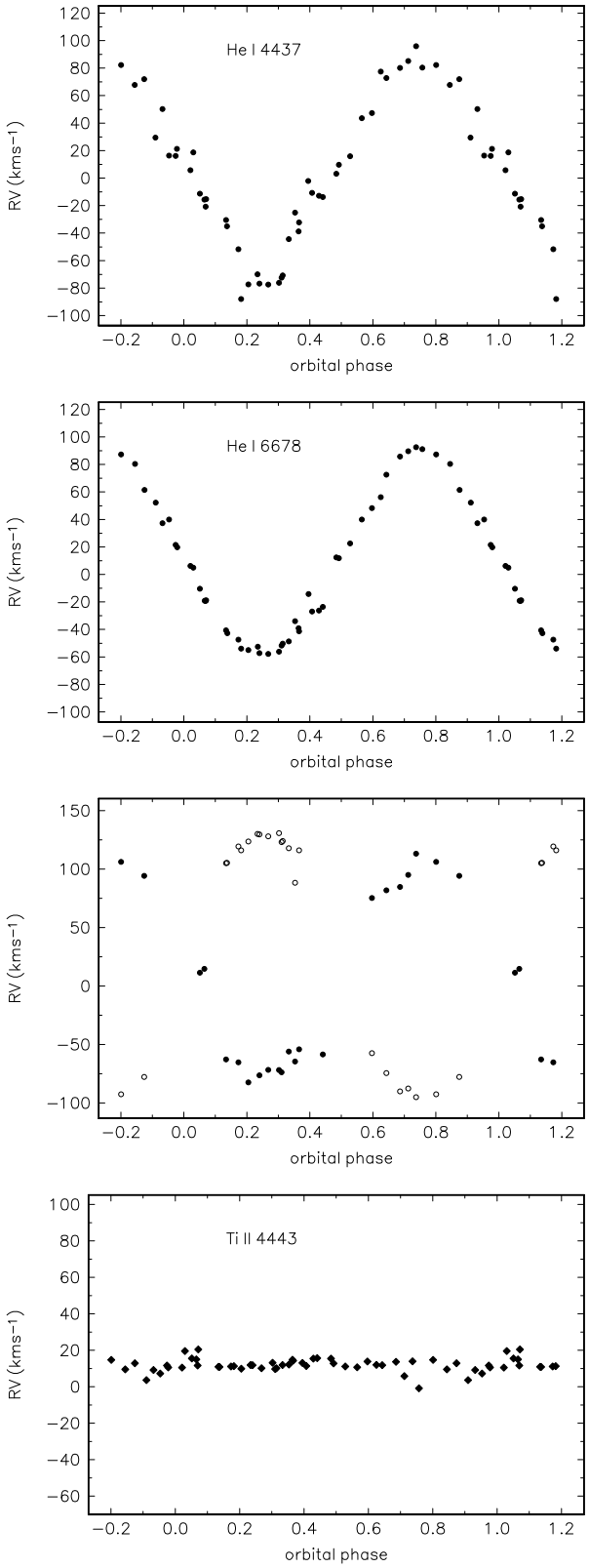

Fig. 4. RV curves of all three components identified in the spectra as measured in SPEFO. *The two upper panels* show the RV curves of the weak He I 4437 Å line and a stronger He I 6678 Å line, which are both only seen for component 1; *the third panel* from the top shows the RVs derived from the Fe II 4549 Å line for components 1 and 2, and *the bottom panel* shows the RVs of the Ti II 4443 Å line of component 3. The RVs of components 1, 2, and 3 (see Fig. 1) are denoted by black dots, open circles, and diamonds, respectively.

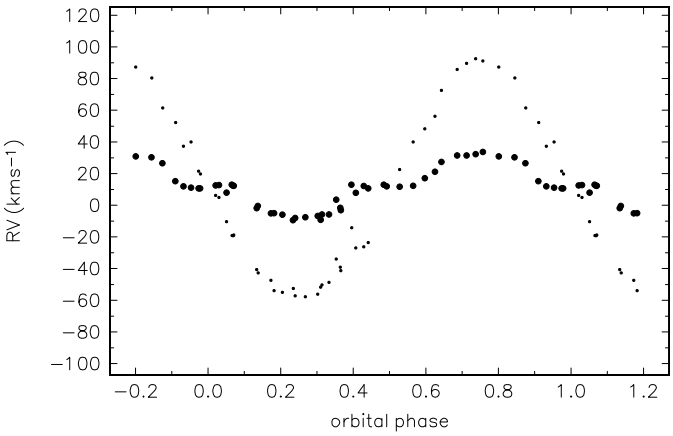

Fig. 5. An apparent orbital variation in the RV of the Hα absorption core measured directly in SPEFO (black circles) is compared to the curve of the He I 6678 Å line, which is only seen for component 1 (dots). See the text for comments.

Table 3. Exploratory orbital solutions obtained with FOTEL for a circular orbit.

Element	He I 6678 Å	He I 4437.551 Å
$T_{\rm min.I}$	0.7078 ± 0.0032	0.7039 ± 0.0035
K_1 (km s^{-1})	72.5 ± 1.2	75.9 ± 3.3
γ (km s^{-1})	14.28 ± 0.80	12.0 ± 1.9
rms (km s^{-1})	5.17	12.3
No. of RVs	44	44

Notes. The orbital period was kept fixed. The epoch of upper conjunction is given in HJD-2 450 545 and rms stands for the rms of 1 observation.

we discuss it in detail in the Appendix, using a simulation with synthetic spectra.

In Table 3, we present a few exploratory orbital solutions based on RVs measured with SPEFO and derived with the program FOTEL (Hadrava 1990, 2004a). We note that the epoch of the upper conjunction agrees with that expected from photometry.

We conclude that there are three possible origins of component 3:

1. circumbinary gas around the close binary;
2. circumstellar gas expelled by one of the components;
3. a third component in a triple system.

We now use different approaches to distinguish these three possibilities and derive reliable orbital elements of the binary.

3.3. Spectra disentangling

It is clear that the complicated shape of the line profiles of the binary makes it difficult to derive accurate RV curves in a classical way. We therefore decided to derive the orbital elements and disentangle individual component spectra using the program KOREL developed by Hadrava (1995, 1997, 2004b), in particular the latest publicly available version dated December 2, 2004.

The preparation of data for the program KOREL deserves a few comments. The electronic spectra at our disposal were recorded with a pixel-to-pixel separation of some 1.9 km s^{-1} in the blue, and about 1.3 km s^{-1} in the red parts of the echelle spectra. Considering this, we therefore rebinned the spectra into equidistant steps in RV, choosing the RV step of 1 km s^{-1} for all spectra not to lose resolution. The rebinning was carried out with the help of the HEC35D program written by PH[1]. In comparison to a similar data preparation program PREKOR by Dr. P. Hadrava, distributed with KOREL, HEC35D allows the user to choose the initial *and* final wavelength and operates on spectra of virtually any length. Like PREKOR, HEC35D derives consecutive discrete wavelengths given by

$$\lambda_n = \lambda_1 \left(1 + \frac{\triangle \mathrm{RV}}{c}\right)^{n-1}, \qquad (2)$$

where λ_1 is the chosen initial wavelength, $\triangle$RV is the constant step in RV between consecutive wavelengths, and λ_n is the wavelength of the nth rebinned pixel. However, the relative fluxes of these new wavelength points are derived using the INTEP program (Hill 1982), which is a modification of the Hermite interpolation formula. It is possible to choose the initial and last wavelength and the program smoothly fills in the rebinned spectra with continuum values of 1.0 at both edges[2].

To take the variable quality of individual spectra into account, we measured their S/N in the line-free regions and assigned each spectrum a weight given by

$$w = \frac{(S/N)^2}{(S/N_{\rm mean})^2},$$

where $S/N_{\rm mean}$ denotes the mean S/N of all spectra. The S/N ranged from about 100 to 600, depending also on the spectral region studied.

We briefly recall that KOREL uses the observed spectra and derives both the orbital elements and the mean individual line profiles of up to five stars. These stars may form a hierarchical system of two mutually orbiting binaries and a distant, also gravitationally bounded fifth star. To be able to disentangle also component 3 present in the line profiles of V945 Cen, we run KOREL formally on the assumption that – besides a binary – there is another distant component (No. 5 in Hadrava's hierarchical system), which has *the same orbital period* as the binary and a negligible semi-amplitude of the orbital motion around the common centre of gravity with the binary. In particular, we set $K_3 = 0.001$ km s^{-1}. This approach is suitable for both the case that the third system of lines belong to a distant third component, and the case that there is a circumstellar envelope around the whole system. We note that our spectra cover an interval of only four days so that the lines of the putative third component would appear stationary over such a short time anyway.

Since V945 Cen is an ellipsoidal variable, we allowed for variable strengths of the spectral lines in individual spectra during the solutions (cf. Hadrava 1997).

Our experience with KOREL is that the result is sensitive to the choice of starting values of the elements and initial values of the simplex steps. This is understandable because the sum of squares of residuals using all data points of individual spectra is very complicated and it is easy to end up in a local minimum. This was clearly illustrated in an excellent study of DW Car by Southworth & Clausen (2007, see their Fig. 3).

[1] The program HEC35D with User's Manual and a few auxiliary programs is available to interested users at ftp://astro.troja.mff.cuni.cz/ftp/hec/HEC35. Reports of possible bugs to P.H. are welcome.

[2] This is necessary since KOREL requires that the number of the input data points is an integer multiple of 512.

To cope with the problem, we first investigated the variation in the sum of squares as a function of *the semi-amplitude of the primary* only, keeping all other elements fixed at values we derived from the FOTEL solution of the photometry and preliminary analyses of the spectra at both elongations. In all of these trial solutions, all three spectra were disentangled. We first derived a solution for the constant strength of the lines and then, in the same run, we allowed the line strengths to vary.

The plot of the sum of squares of residuals as a function of the semi-amplitude K_1 is shown in Fig. 6, separately for the following four stronger lines: Mg II 4481 Å line, Fe II 4549 Å line, Si II 6347 Å line, and He I 6678 Å line. The He I 4471 Å line is not suitable since it has an almost stationary Ti II 4468 Å line in its blue wing. The Hα line was also found to be too complex and was not disentangled. One can see that there are indeed several local minima and the range of plausible values of K_1 varies from one line to another. It is especially instructive for the neighbourhood of the He I 6678 Å line, where any lines from the secondary and the third spectrum are very weak or simply missing. In the end KOREL finds more or less flat continua for the components 2 and 3 but from time to time it suddenly jumps to another, actually deeper minimum. Nevertheless, our direct measurements in SPEFO indicate a semi-amplitude of about 73 km s^{-1}. After inspecting the results for all four lines, we carried out another series of runs to find plausible limits for the mass ratio K_1/K_2, this time keeping K_1 fixed at 73.5 km s^{-1}.

This search was only carried out for the Mg II 4481 Å line, Fe II 4549 Å line, and Si II 6347 Å line since there is no detectable He I 6678 Å line of the secondary. The results of this search are again shown graphically, in Fig. 7. One can again note the different sensitivities of the different lines to the mass ratio but it seems that $K_1/K_2 = 0.70$ reproduces all three lines well.

Fixing the mass ratio, we carried out the final round of trial KOREL solutions, checking whether the third system of lines is stationary or exhibits some periodic RV changes with the binary orbital period. By increasing the value of K_3 from zero to positive values, we always found a higher sum of residuals. We therefore conclude that the RV of the third system of spectral lines was constant over the period of our observations. This can be interpreted in two possible ways. Either the third spectrum represents a real third star, bounded or unbounded to the ellipsoidal binary, or it is a shell spectrum from some kind of envelope around the whole system.

In the final step of our analysis, we derived another set of trial KOREL solutions for the four considered lines and now also for the spectra covering the region containing the He I 4437 Å and He I 4471 Å lines, this time also allowing for the convergency of K_1 and the mass ratio (the latter with the exception of the He I 6678 Å line, of course). We slightly varied the initial values of the elements from their mean values used after the first runs, and also varied the initial steps. For each line, we then adopted the solution with the smallest sum of residuals. The resulting elements from these solutions are summarized in Table 4. Since KOREL does not provide error estimates for the elements, the inspection of Table 4 provides some idea of the uncertainties in the elements. We also imported the disentangled blue spectra of components 1 and 2 into SPEFO and derived the mean systemic velocities from the RV measurements of 9 He I and metallic lines. The results are $\gamma_1 = 14.5 \pm 2.1$ km s^{-1} and $\gamma_2 = 14.6 \pm 1.1$ km s^{-1}. They represent the best estimate of the true systemic velocity of the binary and the excellent mutual agreement of both values shows the quality of the final disentangling.

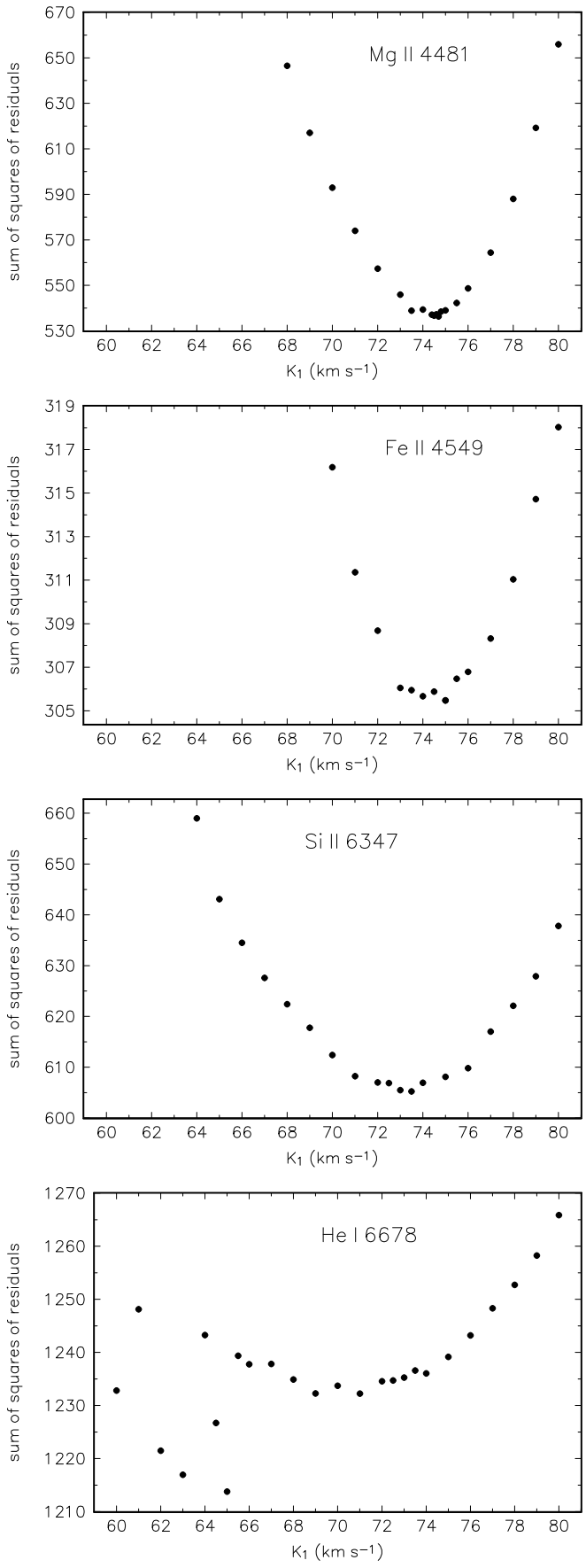

Fig. 6. The sum of squares of residuals of exploratory KOREL solutions as a function of the semi-amplitude of the primary, K_1, derived separately for the four indicated spectral lines. See the text for details.

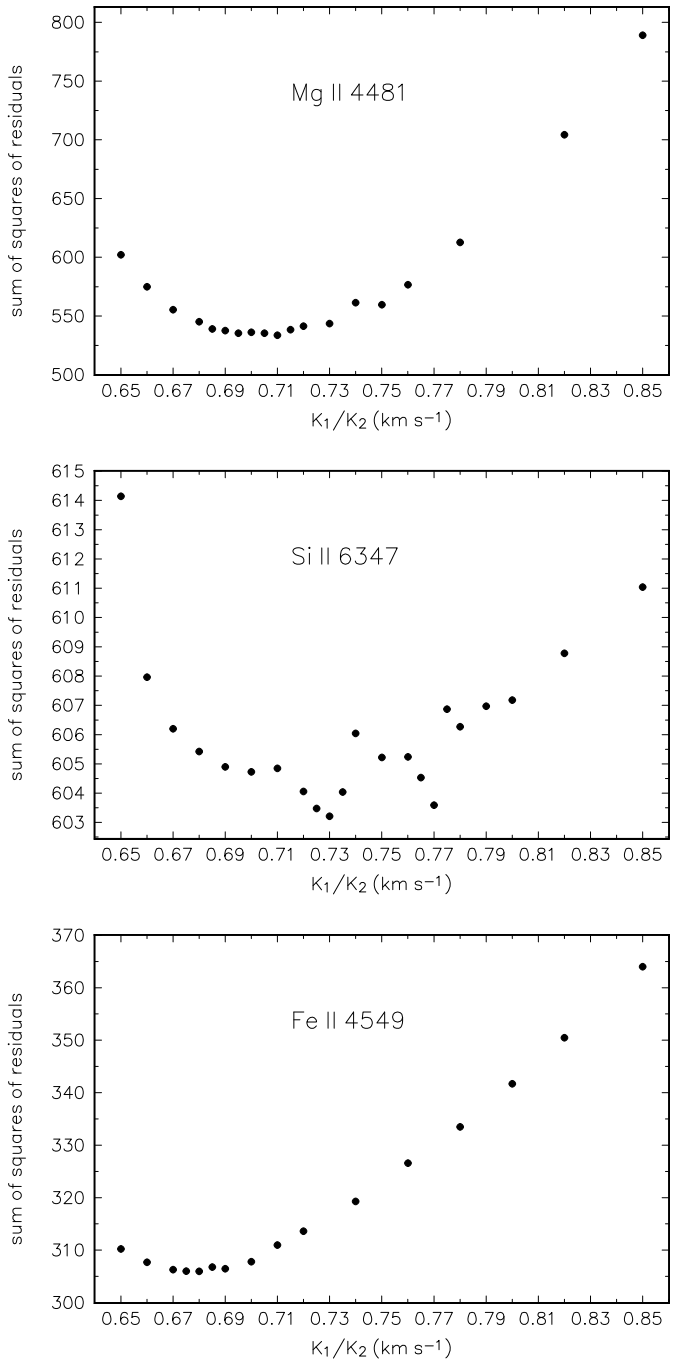

Fig. 7. The sum of squares of residuals of exploratory KOREL solutions as a function of the mass ratio K_1/K_2 derived separately for the Mg II 4481 Å, Si II 6347 Å, and Fe II 4549 Å. See the text for details.

Our ultimate goal is to derive a simultaneous solution combining photometry and spectroscopy and using the program PHOEBE. It is true that KOREL also derives individual radial velocities for individual disentangled spectral components but the accuracy of these RVs depends on the quality of individual spectra. It is easy to verify that if an orbital solution is derived from these RVs (for instance, using the program FOTEL), the result *differs* from the orbital elements derived by KOREL. To constrain PHOEBE to adopt the KOREL orbital elements, we therefore proceeded in a somewhat unusual way. For each individual KOREL solution of Table 4, we derived the model-predicted RVs from KOREL for the HJDs of our 44 spectral observations. We then averaged these RVs from four wavelength segments for each individual spectrum and these average RVs were subsequently used in PHOEBE.

Table 4. Circular-orbit solutions derived with KOREL for several short spectral regions near stronger spectral lines.

Element	He I 4471	Mg II 4481	Fe II 4549	Si II 6347
$T_{\mathrm{Min\,I}}$	0.7068	0.7080	0.7081	0.7086
K_1(km s^{-1})	73.9	75.7	74.0	74.2
K_2(km s^{-1})	102.3	105.5	108.1	100.4
K_1/K_2	0.722	0.718	0.684	0.739

Notes. The period was kept fixed and the epoch of the primary minimum $T_{\mathrm{Min\,I}}$ is tabulated in HJD−2 450 545. Note that by its principle, KOREL does not provide information on the RV zero point in the solution. The only way to derive the systemic velocities of both components is to measure the individual disentangled line profiles in the classical way – see the text for details.

4. Spectrophotometric modeling

To model the light and RV data simultaneously we used PHOEBE 0.32 (Prša & Zwitter 2005), a modeling suite based on the Wilson-Devinney program (Wilson & Devinney 1971). We paid attention to ensuring consistency with SEDs, so that all gravity darkening effects caused by shape distortion follow the Von Zeipel law for radiative envelopes and the limb darkening coefficients are interpolated from the tables. That means that the ratio $T_{\mathrm{eff2}}/T_{\mathrm{eff1}}$ is the only unknown. Specific passband intensities and limb darkening coefficients were computed for the Geneva passbands from Castelli & Kurucz (2004)'s NEWODF models spanning from 3500 K to 50 000 K across the entire H-R diagram. The SED functions were synthetized with SPECTRUM 2.75[3] (Gray & Corbally 1994) at a 1 Å dispersion, from 3000 Å to 10 000 Å. The limb darkening tables were computed by synthetizing SEDs in 20 values of $\mu = \cos\theta$ from the center of the disk to the limb, and fitting the linear cosine law and non-linear log and square root laws by least squares. The computed auxiliary tables are added to the default PHOEBE distribution and are freely available from the PHOEBE homepage.

To obtain an independent estimate of the effective temperatures of individual components, we used PHOEBE's color-constraining technique (Prša & Zwitter 2006). The Cramer & Maeder (1979) parameters X and Y were computed for each observed photometric observation; they were used to obtain a reddening-free effective temperature and effective gravity of the object. Their values are depicted in Fig. 8; there is a slight phase dependence present in parameter X, which is expected because of its dependence on T_{eff} that changes due to ellipsoidal variation. The values obtained in this manner are $T_{\mathrm{eff}} = 12\,390$ K ± 110 K and $\log g = 4.45 \pm 0.02$. Color constraining yields the estimates of individual temperatures to be $T_{\mathrm{eff,1}} = 13\,040$ K ± 84 K and $T_{\mathrm{eff,2}} = 10\,880$ K ± 122 K, in close agreement with spectroscopic determination. Hence we suggest the spectral types of the primary and secondary to be B7 and B8.5, respectively.

Spectroscopic observations of V945 Cen provided RV curves for both components, allowing us to accurately derive the mass ratio q, the projected semi-major axis $a \sin i$, and systemic velocity γ. These values, listed in Table 5, were determined by

[3] http://www.phys.appstate.edu/spectrum/spectrum.html

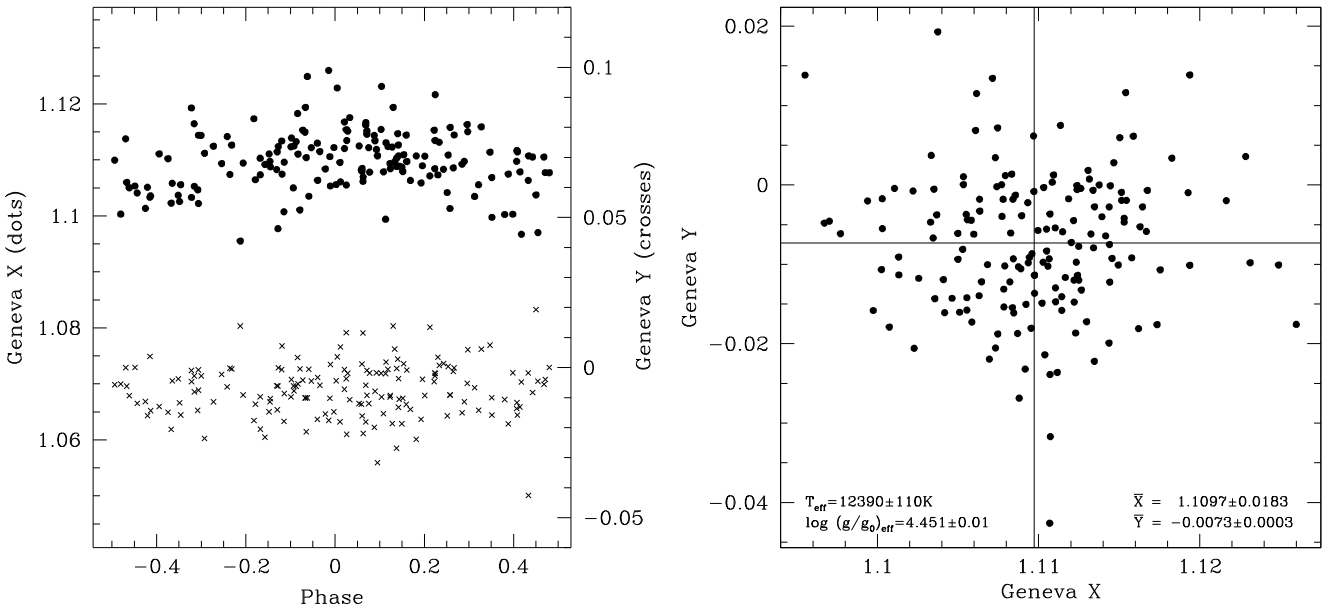

Fig. 8. *Left*: Cramer & Maeder (1979) parameters X (dots) and Y (crosses) of observed data points as a function of phase. There is a slight phase dependence present in parameter X, which is expected due to its dependence on $T_{\rm eff}$. *Right*: the XY parameter plane. The scatter shows that the average values of X and Y parameters are statistically meaningful. This is also true for the values of $T_{\rm eff}$ and $\log g$ obtained from the plot.

Table 5. Physical properties of V945 Cen based on measured RVs.

Parameter:			
$q = M_2/M_1$	0.715	±	0.034
$a \sin i$ [$R_\odot$]	2.29	±	0.11
γ [km s^{-1}]	14.55	±	1.6

Notes. Note that the systemic velocity was derived measuring the disentangled line profiles of 9 unblended lines of the primary and secondary from the blue spectral region in SPEFO.

passing the solution iteratively between KOREL and PHOEBE, and validated by Gaussian fits to spectral lines in SPEFO. The cross-correlation method based on two templates, as implemented in TODCOR (Zucker & Mazeh 1994), provided a fully consistent fit for the primary RV, but failed to properly extract the secondary RV, because of the presence of the third system of spectral lines. Once these parameters were determined from the RV modelling, we kept them fixed throughout the study. The projected semi-major axis value $a \sin i = 2.291\,R_\odot$ was used to constrain the fit: for each value of i, a was computed so that $a \sin i$ remained constant.

Since V945 Cen is an ellipsoidal variable, there is a very strong correlation between the stellar radii and the orbital inclination, which prevents the identification of a unique solution. By considering the two possible interpretations of the third system of spectral lines, we modelled two distinct possibilities: 1) the third source is optically thin and contributes to line blanketing; and 2) the source is optically thick and contributes to the joint continuum as the third light in the system. To find physically plausible boundaries of the parameter space, we performed an i-search from 20° to 35°, adjusting effective potentials (proxies to stellar radii) and the secondary temperature $T_{\rm eff,2}$ for each value of i. The semi-major axis a, the passband luminosities L_i, and the limb darkening coefficients were computed automatically after every iteration. Solid lines in Fig. 9 depict the results with (left) and without (right) the inclusion of the third light. From the cost function profile ($\sum$(O−C)^2; bottom right panel), it is immediately clear that for any inclination above 19° for the model with the third light, and 17° for the model without the third light, *all* solutions are degenerate.

To break this degeneracy, we computed the values of the primary and secondary star surface potential corresponding to the smallest and largest observed radii for B7 and B8.5-type stars, namely $R_{1,\rm min} = 2.2\,R_\odot$, $R_{1,\rm max} = 2.8\,R_\odot$, and $R_{2,\rm min} = 1.6\,R_\odot$, $R_{1,\rm max} = 2.6\,R_\odot$ (Harmanec 1988). These limits are depicted by dash-dotted lines in the upper two panels. The intersection with the model determines the plausible range of radii, hence inclinations for V945 Cen, and is marked by a dark-grey strip on all panels. Finally, the horizontal band limited by the surface potential values at the Lagrange points L_1 and L_2 shows the overcontact region of the parameter space. We conclude that, for both considered models, V945 Cen is a nearly contact, yet still *detached* binary. For the model with the third light, a semi-detached configuration with the primary filling the Roche lobe also appears to be satisfactory, but the mass of the primary that would result from this configuration is unrealistic: $M_1 = 6.47\,M_\odot$ compared to the expected ~3.4 $M_\odot$. Since the secondary-star potential always falls well outside the overcontact region, an overcontact configuration can safely be ruled out.

For the masses of these two stars to be reconciled with the expected masses of the main-sequence B7 and B8.5 stars, the band's upper end inclinations are more suitable: for an inclination of 23° and the implied semi-major axis $a = 5.86\,R_\odot$, the resulting radii $R_1 = 2.2\,R_\odot$ and $R_2 = 1.7\,R_\odot$ and the derived masses $M_1 = 3.73\,M_\odot$ and $M_2 = 2.67\,M_\odot$ are in excellent agreement with those expected (Harmanec 1988). Moreover, the effective temperature of the secondary (~10 650 K and ~10 930 K for the models with the third light and without it, respectively) does not contradict the expected value of ~10 880 K. Because of the degeneracy, there is no way to qualify the correctness of the

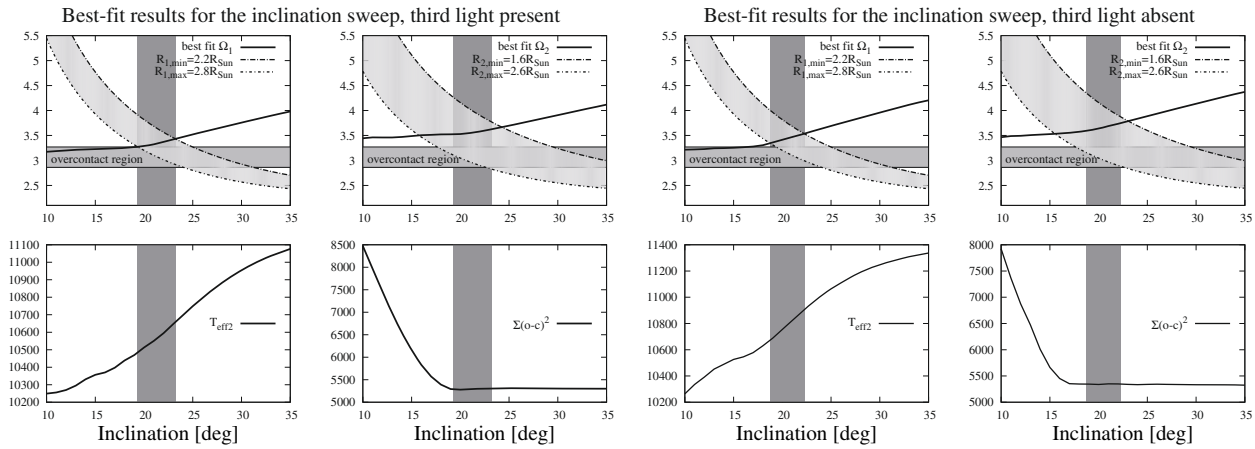

Fig. 9. Boundaries of the physically plausible parameter space. Grid search in inclinations between 10° and 35° was performed and a best-fit solution was obtained for each inclination – depicted by a solid line. The limiting values of the radii for both stars were taken from Harmanec (1988) and used to form a range of allowed values – depicted by a light-grey area. Part of the parameter space corresponding to the overcontact morphology is depicted by a horizontal grey band; solutions below this region overflow L_2 and are physically implausible. The intersection between the model solution and allowed radii is depicted by a dark-grey vertical band on all panels; it represents the range of inclinations that are plausible. The two leftmost panels correspond to the model with third light present, while the two rightmost panels correspond to the model with third light absent.

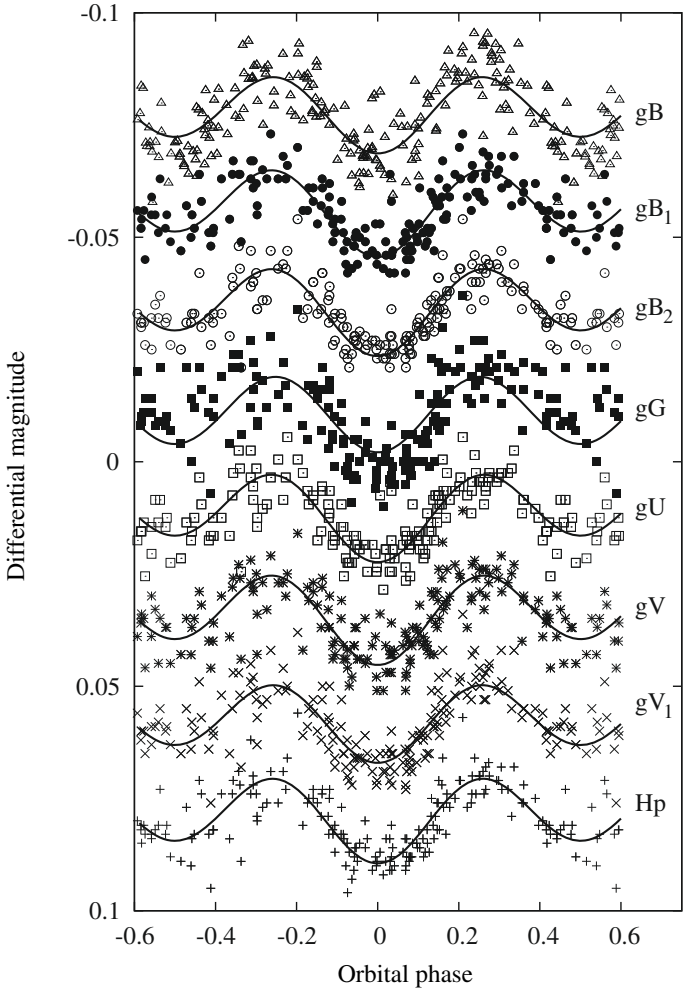

Fig. 10. V945 Cen light curves and a model solution in the absence of third light. For clarity, individual curves are shifted along the ordinate and shown by different symbols. There is a notable discrepancy in the Geneva U passband due to systematic calibration issues in the Balmer jump region.

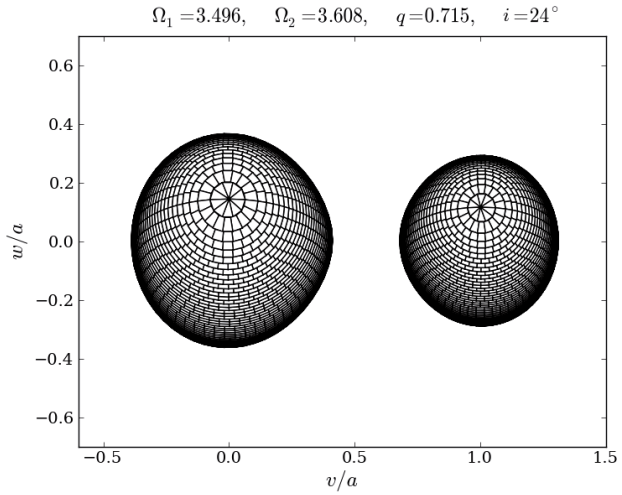

Fig. 11. A diagram showing the geometry of binary components as seen by an observer on Earth. The system is close but still well detached.

model beyond these plausibility estimates; we thus refer to the solution as *probable*, and *discourage the use of these values for calibration purposes as they would lead to a circular argument*.

Figure 11 that illustrates the geometrical configuration of the binary, as seen projected onto the sky, follows from our model. The binary is close but still well detached.

To examine the plausibility of both solutions further, we overplotted the modeled components in the $\log L/L_\odot$-$\log T_{\rm eff}$ diagram (cf. Fig. 12). The depicted theoretical evolutionary tracks for $M = 2.0\,M_\odot$, $M = 2.5\,M_\odot$, $M = 3.0\,M_\odot$ and $M = 3.5\,M_\odot$ were adopted from the Padova stellar evolution models (Marigo et al. 2008) and a log-normal initial mass function (Chabrier 2001). The main plot shows the tracks and the model solutions with and without a third light contribution as pluses and crosses, respectively. The location of the primary star on the diagram coincides for both models because of the adopted $T_{\rm eff,1} = 13\,000$ K, but the inferred masses are different: $M_1 = 3.29 \pm 0.02\,M_\odot$ from the evolutionary tracks agrees well

Table 6. Probable V945 Cen model parameters and their formal error estimates, where Ω is the value of the Roche-model potential used in the WD program, and L_i are the relative luminosities of the components in individual photometric passbands.

Parameter:		Solution in the absence of 3rd light: Primary	Secondary	Solution in the presence of 3rd light: Primary		Secondary
a	($R_\odot$)	5.86 ± 0.21		5.63 ± 0.18		
i	(°)	23.0*		24.0*		
Ω		3.625 ± 0.018	3.695 ± 0.012	3.496 ± 0.024		3.608 ± 0.015
$T_{\rm eff}$	(K)	13000*	10930 ± 40	13000*		10687 ± 52
M	($M_\odot$)	3.74 ± 0.58	2.67 ± 0.54	3.32 ± 0.51		2.37 ± 0.48
R	($R_\odot$)	2.20 ± 0.09	1.73 ± 0.07	2.09 ± 0.12		1.67 ± 0.09
L	($L_\odot$)	123 ± 20	35 ± 6	111 ± 21		37 ± 7
$M_{\rm bol}$	(mag)	−0.50 ± 0.2	0.87 ± 0.2	−0.38 ± 0.2		0.95 ± 0.2
log g	[cgs]	4.3 ± 0.1	4.4 ± 0.1	4.3 ± 0.1		4.4 ± 0.1
L_i	B band	0.684	0.316	0.534	0.227	0.239
L_i	$B1$ band	0.688	0.312	0.536	0.223	0.241
L_i	$B2$ band	0.679	0.321	0.530	0.232	0.238
L_i	G band	0.667	0.333	0.517	0.242	0.242
L_i	U band	0.749	0.251	0.620	0.184	0.197
L_i	V band	0.669	0.331	0.519	0.240	0.241
L_i	$V1$ band	0.670	0.330	0.520	0.240	0.240
L_i	Hp band	0.679	0.321	0.529	0.232	0.239

Notes. They are normalized in such a way that $L_1 + L_2 = 1$ for the first model without the third light, and $L_1 + L_2 + L_3 = 1$ for the triple-star model. Note that for this model, the values of L_3 are tabulated in the central column between the primary and secondary.
* Values denoted with an asterisk are *fixed*.

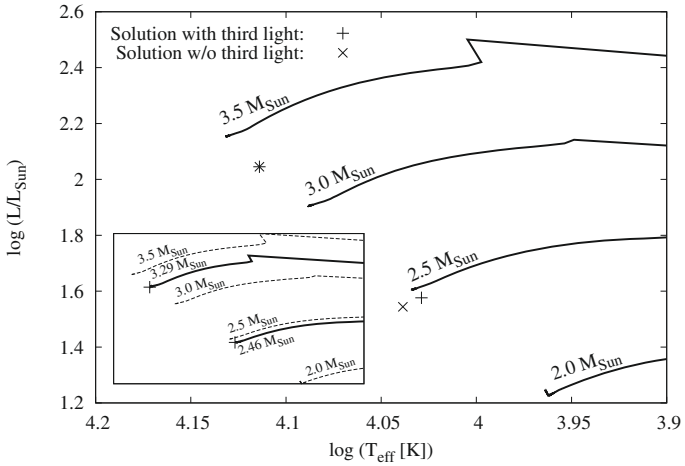

Fig. 12. Evolutionary tracks compared with the components of V945 Cen. Solid lines on the main plot show tracks computed with the Padova evolution code for the initial mass of $M = 2.0\,M_\odot$, $M = 2.5\,M_\odot$, $M = 3.0\,M_\odot$, and $M = 3.5\,M_\odot$. The inset depicts the closest tracks for the solution with a third light component: $M_1 = 3.29 \pm 0.02\,M_\odot$ and $M_2 = 2.46 \pm 0.02\,M_\odot$. Both stars yield a consistent age of ∼10 million years, at or very close to the ZAMS. The masses are in good agreement with their spectrophotometric counterparts, $M_1 = 3.32 \pm 0.51\,M_\odot$ and $M_2 = 2.37 \pm 0.48\,M_\odot$. For the solution without third light, the tracks yield masses that are a bit more discrepant, yet still well within the error bars of their spectrophotometric counterparts. Evolutionary tracks thus slightly favour the third light-contaminated model and, hence, a true stellar source of the third spectrum.

with the third-light contaminated model ($M_1 = 3.32 \pm 0.51\,M_\odot$), but only marginally well with the model without the third light ($M_1 = 3.74 \pm 0.58\,M_\odot$). The location of the secondary star for both models differs slightly and constrains the probable nature of the third spectrum. Namely, for the model with the third light, the mass of the secondary inferred from the tracks is $M_2 = 2.46 \pm 0.02\,M_\odot$ (see the inset in Fig. 12), in good agreement with the adopted spectrophotometric value $M_2 = 2.37 \pm 0.48\,M_\odot$. For the model without the third light and the modeled spectrophotometric value of $M_2 = 2.67 \pm 0.54\,M_\odot$, the evolution-inferred value of $M_2 = 2.45 \pm 0.02\,M_\odot$, although somewhat discrepant, is still well within the error bars. Finally, the model with the third light predicts both components to be at (or very close to) the zero-age main sequence (ZAMS) with an age of ∼10 million years. The model without the third light, however, predicts the secondary star temperature to be by ∼300 K too hot for the ZAMS. Based on these observations, it seems that a real third star is present in the system.

5. Conclusion

In this study, we have discovered that the bright variable star V945 Cen is a short-period, nearly contact double-lined spectroscopic binary with pronounced ellipsoidal variations. We derived the basic physical properties of the system from multicolor photometry and high-resolution spectroscopy. We also detected a strong and seemingly stationary third B-type line spectrum. Although the arguments presented in Sects. 2.3 and 4 strongly favour the presence of a real third body in the system, interferometric or high-precision astrometric observations would provide the final resolution of this issue and are strongly encouraged. In addition, future spectroscopic observations may allow the detection of measurable RV variations in the third spectrum and also a secular change in the systemic velocity of the close binary as the pair and the tertiary would move in the orbit around the common centre of gravity.

Acknowledgements. We thank Peter De Cat, Joris De Ridder and Gwendolyn Meeus from the Institute of Astronomy of the K.U. Leuven, who obtained some photometric observations of V945 Cen during the long-term monitoring program. We acknowledge the use of the programs FOTEL and KOREL, made publicly available by their author, Dr. Petr Hadrava. Comments by an anonymous referee helped to improve the presentation. The research of P.H. was supported by the grants 205/03/0788, 205/06/0304, 205/08/H005, and in the final stages also P209/10/0715 of the Czech Science Foundation and also from the Research Program MSM0021620860 *Physical study of objects and processes in*

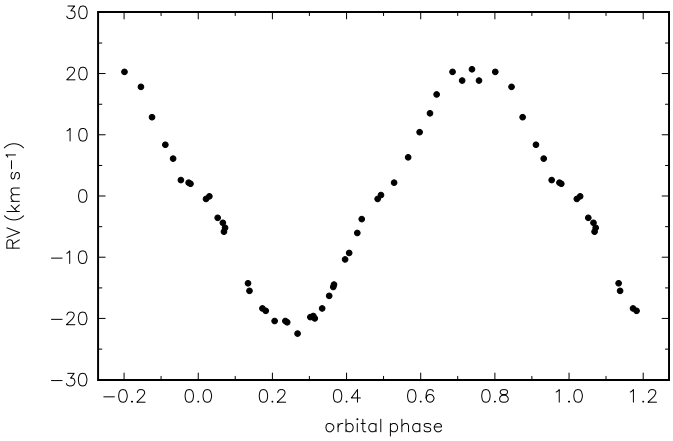

Fig. A.1. The RV of the Hα absorption core measured in SPEFO in a series of artificially created synthetic spectra. See the text for details.

the solar system and in astrophysics of the Ministry of Education of the Czech Republic. The Leuven authors are supported by the Research Council of K.U. Leuven under grant GOA/2008/04. We acknowledge the use of the electronic database from CDS Strasbourg and electronic bibliography maintained by the NASA/ADS system.

Appendix A: Simulation of a spurious RV variation resulting from a blend of three spectra

As we have shown in this study, the observed spectrum of V945 Cen is a sum of three spectra: two late B spectra of the binary components revolving around each other with a period of $0\overset{d}{.}649$, and a stationary late-B line spectrum from a probable tertiary in the system. In this temperature range, the Hα profiles have very extended Stark-broadened wings and sharp cores. We measured the RV of the Hα core in the observed spectra manually, comparing the direct and flipped profiles of the core in SPEFO. We obtained a RV variation reminiscent of a sum of two sinusoids. One has a period equal to the orbital period of the binary and the other one a period three times shorter (cf. Fig. 5). Our conclusion was that this RV variation is spurious and arises from a strong blending of all three spectra involved.

To carry out a conclusive test that such an apparent RV variation can indeed originate from a blend of a stationary shell line with two spectra of an orbiting binary, we simulated such a situation with the help of synthetic profiles. We used synthetic spectra computed from Castelli & Kurucz (2004)'s NEWODF models, rotated them to 70, 55, and 30 km s^{-1}, Doppler-shifted them according to the mid-exposure times of 44 observed spectra, and merged them with the appropriate relative strengths. We then rectified the resulting composite spectra in SPEFO and measured the RV of the absorption core, as we did for the real data.

The result is shown in Fig. A.1. The similarity with the RV curve obtained from the real Hα profiles is obvious. We note that this finding represents a very important *methodological warning*: if one is unaware of the presence of a third spectrum and carries out similar measurements on the observed spectra, one may conclude that the object is a pulsating star or at least a multiperiodic variable.

References

Aerts, C., & Kolenberg, K. 2005, A&A, 431, 615
Aerts, C., De Cat, P., Peeters, E., et al. 1999, A&A, 343, 872
Briquet, M., Aerts, C., Lüftinger, T., et al. 2004, A&A, 413, 273
Brown, A. G. A., & Verschueren, W. 1997, A&A, 319, 811
Castelli, F., & Kurucz, R. L. 2004, A&A, in Modelling of Stellar Atmospheres, ed. N. Piskunov et al., Poster A20, IAU Symp., 210 [arXiv:astro-ph/0405087]
Chabrier, G. 2001, ApJ, 554, 1274
Cramer, N., & Maeder, A. 1979, A&A, 78, 305
De Cat, P., & Aerts, C. 2002, A&A, 393, 965
De Cat, P., Aerts, C., De Ridder, J., et al. 2000, A&A, 355, 1015
Eyer, L., & Grenon, M. 1997, in Hipparcos – Venice '97, ESA SP-402, 467
Gray, R. O., & Corbally, C. J. 1994, AJ, 107, 742
Hadrava, P. 1990, Contr. Astron. Obs. Skalnaté Pleso, 20, 23
Hadrava, P. 1995, A&AS, 114, 393
Hadrava, P. 1997, A&AS, 122, 581
Hadrava, P. 2004a, Publ. Astron. Inst. Acad. Sci. Czech Rep., 92, 1
Hadrava, P. 2004b, Publ. Astron. Inst. Acad. Sci. Czech Rep., 92, 15
Harmanec, P. 1988, BAC, 39, 329
Hill, G. 1982, Publ. Dom. Astrophys. Obs. Victoria, 16, 67
Horn, J., Kubat, J., Harmanec, P., et al. 1996, A&A, 309, 521
Kazarovets, A. V., Samus, N. N., Durlevich, O. V., et al. 1999, Inf. Bull. Var. Stars No., 4659, 1
Kurucz, R. L. 1979, ApJS, 40, 1
Lenzen, R., Hartung, M., Brandner, W., et al. 2003, in SPIE Conf. Ser., Presented at the Society of Photo-Optical Instrumentation Engineers (SPIE) Conf., ed. M. Iye, & A. F. M. Moorwood, 4841, 944
Marigo, P., Girardi, L., Bressan, A., et al. 2008, A&A, 482, 883
Mathias, P., Aerts, C., Briquet, M., et al. 2001, A&A, 379, 905
Perryman, M. A. C., & ESA. 1997, The HIPPARCOS and TYCHO catalogues, Astrometric and photometric star catalogues derived from the ESA HIPPARCOS Space Astrometry Mission (Noordwijk, Netherlands: ESA Publications Division), ESA SP Ser., 1200
Prša, A., & Zwitter, T. 2005, ApJ, 628, 426
Prša, A., & Zwitter, T. 2006, Ap&SS, 304, 347
Rousset, G., Lacombe, F., Puget, P., et al. 2003, in SPIE Conf. Ser. Presented at the Society of Photo-Optical Instrumentation Engineers (SPIE) Conf., ed. P. L. Wizinowich, & D. Bonaccini, 4839, 140
Škoda, P. 1996, in Astronomical Data Analysis Software and Systems V, ASP Conf. Ser., 101, 187
Southworth, J., & Clausen, J. 2007, A&A, 461, 1077
Waelkens, C., Aerts, C., Kestens, E., Grenon, M., & Eyer, L. 1998, A&A, 330, 215
Wilson, R. E., & Devinney, E. J. 1971, ApJ, 166, 605
Zucker, S., & Mazeh, T. 1994, ApJ, 420, 806